The Meteoritical Society

Meteoritics & Planetary Science 42, Nr 4/5, 811–827 (2007)
Abstract available online at http://meteoritics.org

Petrography and shock-related remagnetization of pyrrhotite in drill cores from the Bosumtwi Impact Crater Drilling Project, Ghana

Agnes KONTNY[1*], Tiiu ELBRA[2], Jana JUST[1], Lauri J. PESONEN[2], Anja M. SCHLEICHER[3], and Jochen ZOLK[1]

[1]Geologisch-Paläontologisches Institut, Ruprecht-Karls Universität, Im Neuenheimer Feld 234, D-69120 Heidelberg, Germany
[2]Division of Geophysics, Department of Physical Sciences, University of Helsinki, P.O. Box 64, FIN-00014 Helsinki, Finland
[3]Department of Geological Sciences, University of Michigan, 1100 North University Avenue, Ann Arbor, Michigan 48109–1063, USA
[*]Corresponding author. E-mail: agnes.kontny@urz.uni-heidelberg.de

(Received 31 July 2006; revision accepted 13 January 2007)

Abstract–Rock magnetic and magnetic mineralogy data are presented from the International Continental Scientific Drilling Program (ICDP) drill cores LB-07A and LB-08A of the Bosumtwi impact structure in order to understand the magnetic behavior of impact and target lithologies and their impact-related remagnetization mechanism. Basic data for the interpretation of the magnetic anomaly patterns and the magnetic borehole measurements as well as for new magnetic modeling are provided. Magnetic susceptibility (150–500 × 10^{-6} SI) and natural remanent magnetization (10^{-3}–10^{-1} A/m) are generally weak, but locally higher values up to 10.6 × 10^{-3} SI and 43 A/m occur. Sixty-three percent of the investigated rock specimens show *Q* values above 1 indicating that remanence clearly dominates over induced magnetization, which is a typical feature of impact structures. Ferrimagnetic pyrrhotite is the main magnetite phase, which occurs besides minor magnetite and a magnetic phase with a Curie temperature between 330 and 350 °C, interpreted as anomalous pyrrhotite. Coercive forces are between 20 and 40 mT. Brecciation and fracturing of pyrrhotite is a common feature confirming its pre-impact origin. Grain sizes of pyrrhotite show a large variation but the numerous stress-induced nanostructures observable by transmission electron microscopy (TEM) are assumed to behave as single-domain grains. We suggest that the drilled rocks lost their pre-shock remanence memory during the shock event and acquired a new, stable remanence during shock-induced grain size reduction. The observed brittle microstructures indicate temperatures not higher than 250 °C, which is below the Curie temperature of ferrimagnetic pyrrhotite (310 °C).

INTRODUCTION

The complex terrestrial impact crater at Lake Bosumtwi in Ghana (06°32′N, 01°25′W) is the youngest (~1.07 Myr old) and best-preserved of about 95 terrestrial impact structures without modification of the crater morphology (Karp et al. 2004). It has a diameter of ~10.5 km with a central uplift of about 1.9 km in diameter and has formed in continental crystalline target rocks with an age of 2.1 Gyr. The Bosumtwi Crater Drilling Project (BCDP), supported by the International Continental Scientific Drilling Program (ICDP), provides core samples of the impact and crystalline basement lithologies from two boreholes (LB-07A and LB-08A) down to a depth of 540 and 450 m, respectively. According to seismic profiles (Scholz et al. 2002), the boreholes were drilled through lake sediments into the crater uplift (LB-08A), and into the annular moat northwest of the central uplift (LB-07A; see Fig. 1 of Deutsch et al. 2007). One of the main interests of the project is to obtain a complete record of impactites at the central uplift and in the crater moat of this largest young impact structure known on Earth to understand the formation and effects of medium-sized impact craters (Koeberl et al. 2006).

The Bosumtwi crater shows high-amplitude and high-frequency airborne magnetic anomalies northeast and southwest of the impact structure (Pesonen et al. 2003). According to surface investigations, magnetite (primary) and hematite (secondary) were suggested as carriers of natural remanent magnetization. It was assumed that a magnetization due to impact-related post-shock thermochemical processes and subsequent alteration occurred. In a review paper on the magnetization of rocks from terrestrial impact craters, Ugalde et al. (2005) summarized different sources of magnetic anomalies based on numerical modeling. As principle

mechanisms they suggested rock melting and recrystallization of new magnetic carriers, magnetic resetting due to temperatures higher than the Curie temperature, remanence demagnetization due to shock and magnetic carrier modification due to hydrothermal processes. The effect of these different processes depends on pressures and temperatures and is related to changing depth and distance from the impact.

These different mechanisms can modify the original remanent magnetization of impact rocks or remagnetize them. In general, the highest magnetization is created by thermal remanent magnetization (TRM). Moderate magnetizations are related to shock-induced remanent magnetization (SRM) and chemical remanent magnetization (CRM). Plado et al. (2000) suggested that a TRM, related to melt rocks from Fe-rich target lithologies (up to 9.2 wt% Fe_2O_3), is able to acquire high and multicomponent natural remanent magnetization and cause the high central negative anomaly over the Bosumtwi structure. Surprisingly, melt rocks are only represented by the suevite unit in drill core LB-07A and some suevite dikes in drill core LB-08A (see Koeberl et al. 2007). Furthermore, pyrrhotite rather than Fe oxides is the main carrier of the magnetic properties (this work; Elbra et al. 2007).

Our study contributes to rock magnetic and magnetic mineralogy data of the drilled lithologies, which provide data for the interpretation of the magnetic anomaly patterns and the magnetic borehole measurements (see also Elbra et al. 2007; Ugalde et al. 2007a, 2007b). Such data contribute to the understanding of the formation of magnetic minerals and the mechanisms creating and modifying magnetic properties like the remanent magnetization and magnetic susceptibility during impact-related processes. Furthermore, we focus on the microstructures of pyrrhotite and propose a remagnetization mechanism for the Bosumtwi impact lithologies.

Geology and Petrography

The Bosumtwi crater was excavated into 2.1–2.2 Gyr old, lower greenschist-facies metamorphic rocks of the Birimian Supergroup, which consists of volcano-sedimentary sequences with slates, phyllites, schists, meta-graywackes, and metavolcanic rocks (including lavas and pyroclastic rocks) (Taylor et al. 1992; Hirdes et al. 1996). The local geology around the Bosumtwi crater is dominated by meta-graywackes composed of quartz, calcite, muscovite, illite, and ferroan clinochlore and quartzitic rocks. In the northeastern and southern sectors, shales attain some importance. In addition to metasediments and metavolcanics, several Proterozoic granitic intrusions occur in the region around the crater (see Fig. 1 of Deutsch et al. 2007). Suevite, which is an impact breccia composed of angular fragments of different rock types as well as glass inclusions, occurs as large blocks of up to several meters wide and as patchy massive deposits outside and north of the crater rim (e.g., Koeberl et al. 1997). Outcrops of suevitic breccias from the Bosumtwi crater were found ~2.7–3.5 km north from the lake, covering an area of about 1.5 km^2, with a thickness of about 10 m. They contain melt shards and rock clasts (meta-graywackes, staurolith-bearing phyllites and mica schists, granites) up to about 40 cm in size, with meta-graywacke dominating (Boamah and Koeberl 2003). Petrographic shock indicators are diaplectic glass, coesite, and planar deformation features (PDFs) in quartz.

Stratigraphic and petrographic descriptions of the two BCDP drill cores LB-07A and LB-08A are given in Coney et al. (2006), Deutsch et al. (2006), Reimold et al. (2006), Deutsch et al. (2007), and Koeberl et al. (2007). In the drill core of LB-08A, the bedrock transition from the meta-graywacke and metapelite unit into the impact breccia occurs at 262 m. In the drill core of LB-07A, this transition is not defined, although below 470 m only metasediments occur. Reimold et al. (2006) interpret these metasediment-rich zones as mega-clasts within the breccia interval. In both drill cores, the bedrock units are transected by suevitic dikes at different depth.

The impact breccia units are subdivided in polymict lithic breccia (Fig. 1a), suevite, monomict lithic breccia, and suevite dikes. In general, meta-graywacke clasts dominate in all breccia units, followed by different proportions of slate, shale, phyllite, schist, and quartzite.

The rocks mostly show a distinct foliation with alternating layers of bright, micaceous (+plagioclase, ±biotite) and dark, chlorite-rich bands. Parallel to these bands ilmenite is often decomposed to leucoxene or rutile and minor pyrrhotite (Fig. 1c). Sulfides (pyrite, pyrrhotite, and chalcopyrite) occur within the foliation planes. Our X-ray diffraction (XRD) studies have shown that quartz, albite, orthoclase, calcite, illite, and Fe-Mg chlorite are the main components in the impact breccias. The geochemical composition from 15 samples of the breccia units is 53–82 wt% SiO_2, 8–20.5 wt% Al_2O_3, 2–9 wt% Fe_2O_3, 0.6–3.5 wt% MgO, 0.2–2.8 wt% CaO, 2.2–4.4 wt% Na_2O, 0.7–2.7 wt% K_2O, and 0.2–0.8 wt% TiO_2. MnO is below 0.08 wt% in all analyzed samples. Two of the analyzed samples (LB-07A: 376.0 and 380.87 m, see also Table 3) show a mafic composition with 44–52 wt% SiO_2, 7–12.5 wt% Al_2O_3, 6.3–9.8 wt% Fe_2O_3, 14.6–14.9 wt% MgO, 0.2–4.1 wt% CaO, 0.04–0.4 wt% Na_2O, 0.04–0.1 wt% K_2O, 0.3–0.5 wt% TiO_2, and 950–1400 ppm Ni. This rock, classified as greenschist, is composed of quartz, Mg-rich chlorite, albite, dolomite, and magnesite. It occurs as clasts within the polymict lithic breccia unit. Interestingly, this rock contains Fe-, Ni-, Co-, and As-bearing sulfides (Fig. 1b) only in lenses but rarely in the rock matrix.

According to Morrow (2006), shock-metamorphic features in quartz from the drill cores are 1) irregular subplanar

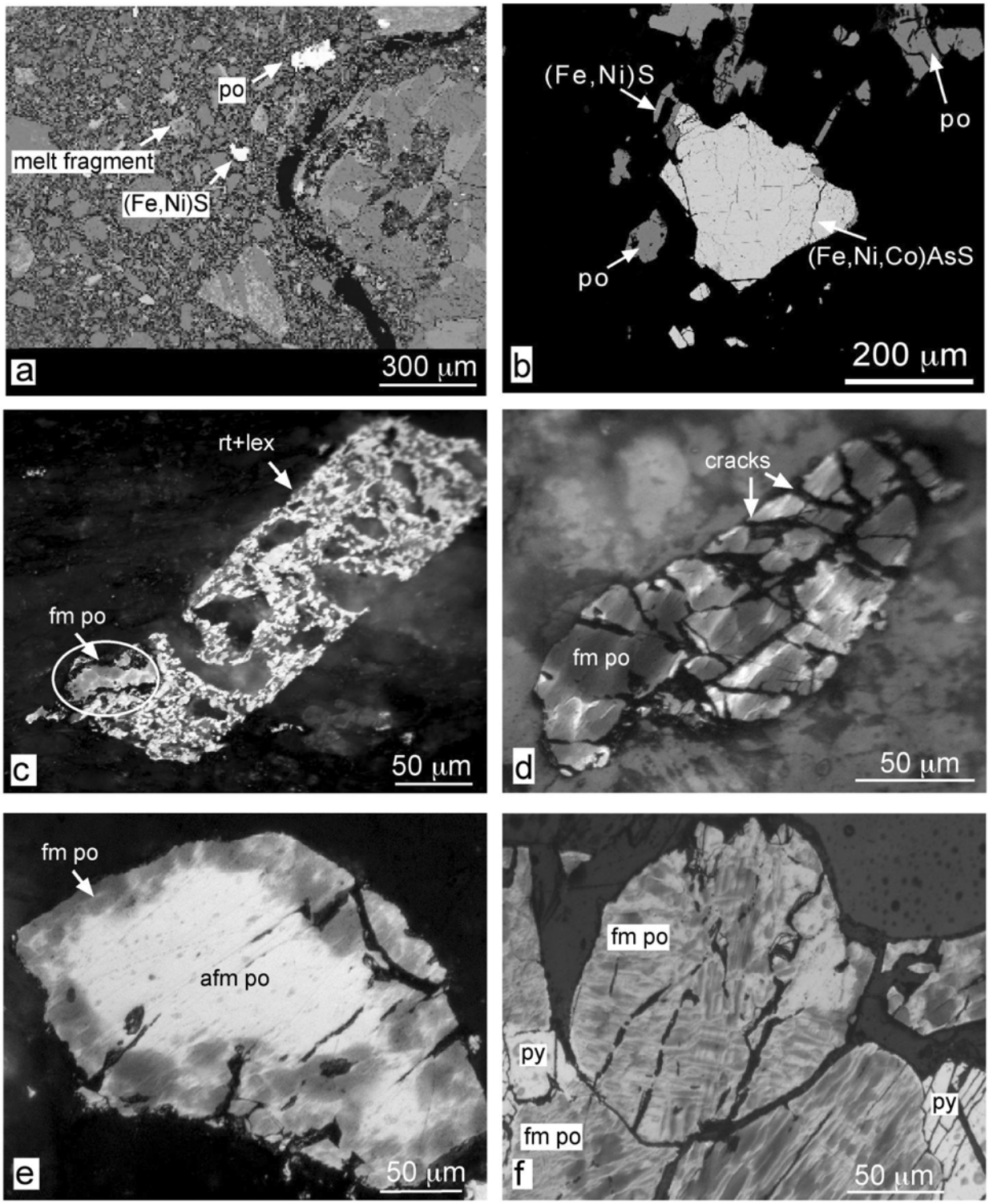

Fig. 1. Photomicrographs with pyrrhotite from different depth and lithology of the LB-07A drill core. a) A BSE image shows the varying size of angular fragments consisting of rock clasts, melt shreds, and mineral grains in a polymict lithic breccia at 354.20 m (po = pyrrhotite). b) A BSE image of pyrrhotite grains associated with millerite [(Fe,Ni)S] and sulfoarsenide [(Fe,Ni,Co)AsS] in a sulfide lens within a greenschist-clast at 376.0 m (polymict breccia unit). c) Ferrimagnetic pyrrhotite (fm po) next to rutile and leucoxene (bright gray) as alteration products of ilmenite in a clast from the suevite at 389.73 m. d) Fractured ferrimagnetic pyrrhotite in a clast from the suevite at 408.49 m. e) Ferrimagnetic pyrrhotite as rim around antiferromagnetic type (afm po). Note the abundant cracks in the grain (polymict lithic breccia, 354.20 m. f) Brecciated ferrimagnetic pyrrhotite in a polymict lithic breccia, 356.32 m. (c to f) are coated with a magnetic colloid to distinguish magnetic from non-magnetic phases.

and curvilinear fractures, 2) grain mosaicism and irregular undulous extinction, 3) "toasted" regions within grains containing abundant fluid-inclusions, often associated with denser concentrations of planar fractures and PDFs with up to three sets, 4) diaplectic glass, evidenced by optically isotropic grains, and 5) few optically high relief crystals, which may potentially be the high-pressure polymorphs stishovite or coesite. According to shock petrographic features, Reimold et al. (2006) and Deutsch et al. (2007) attribute the impact breccias of the two drill cores to the <26 GPa shock zone. As a consequence of these relatively low peak-shock pressures, annealing was estimated only at low temperatures.

METHODS

Sixty drill-core samples from LB-07A and LB-08A were treated with epoxi-resin because of the fragile impactite samples. Two to four cylindrical specimens with a sample volume of ~1.8 cm^3 were drilled from each sample. From these cylinders the natural remanent magnetization, magnetic susceptibility (χ, see also Elbra et al. 2007), and its field-dependence in twenty-one intensities from 2 to 450 A/m were measured. A field-dependence parameter (χ_{Hd}) was calculated (Table 3) according to the formula $\chi_{Hd} = (\chi_{300A/m} - \chi_{30A/m})/\chi_{300A/m} \times 100$ given by de Wall (2000). Thirty and 300 A/m indicate the field, at which the magnetic susceptibility is measured. Detailed information on the field-dependence of magnetic susceptibility is also given in Vahle and Kontny (2005).

Magnetic carriers of the rocks were identified using the temperature-dependence of low-field magnetic susceptibility (χ–T), and the stepwise thermal demagnetization of natural remanent magnetization (NRM). The χ–T measurements were done in the temperature range –192 to 700 °C for ~30 samples at the Geological-Palaeontological Institute, University of Heidelberg, and for ~30 samples at the Division of Geophysics, University of Helsinki, using a KLY-2, KLY3S or KLY4S kappabridge, combined with a CS-2 or CS-3 and CS-L furnace apparatus of AGICO (Hrouda 1994). Determination of NRM unblocking temperatures was done by thermal demagnetization of NRM with progressive heating from room temperature to 550 or 700 °C in zero-field. Stepwise alternating field (AF) demagnetization of NRM was performed in twelve steps of different AF intensities: 2.5, 5.0, 7.5, 10, 20, 30, 40, 50, 75, 100, 130, and 160 mT, using a MI AFD 1.1 demagnetizer (Magnon International). Stepwise heating of the samples to a temperature of 550 °C was performed using the thermal demagnetizer MMTD1. Remanence measurements between each AF and thermal step were performed on a JR-5A spinner magnetometer (AGICO). Hysteresis parameters were measured on a vibrating sample magnetometer (Princeton Measurements, 3900 VSM) in Helsinki. These data were normalized by mass and background was subtracted.

The minerals were identified using an optical polarizing microscope (Leitz Orthoplan) in transmitted and reflected light and backscattered electron images (BSE) were undertaken on carbon-coated polished thin sections with a LEO 440 scanning electron microscope (SEM) at the Institute for Environmental Geochemistry of the University of Heidelberg. Qualitative analyses of mineral composition were obtained by energy dispersive spectroscopy (EDS; Link Isis 300, Oxford) with an acceleration voltage of 20 kV. XRD analyses of whole rock samples were done using a D500 diffractometer at the Geological-Palaeontological Institute. Electron microprobe analyses were made with a Cameca SX 51 at the Mineralogical Institute in Heidelberg. An accelerating voltage of 20 kV and a sample current of 20 nA were used. Pyrite (for Fe and S), niccolite (for Ni), and pure metals (for Co) were used as standards.

The real nature of deformation features in pyrrhotite can only be resolved by transmission electron microscopy (TEM). Four key samples were therefore selected and investigated using a Philips CM12 TEM housed at the electron microbeam analytical laboratory (EMAL), University of Michigan, USA. Thin sections ~100 μm in thickness were prepared and small Cu-washers (1 mm in diameter) adhered to the pyrrhotite-bearing portions of the sections. The samples were ion-milled with a GATAN PIPS until small holes were visible, and mapped for pyrrhotite using a SEM Hitachi S3200N. The TEM was equipped with a Kevex Quantum solid-state detector (120 kV, 20 mA) and qualitative chemical analyses were obtained in scanning TEM mode using a beam diameter of 5 nm and a scanning area of 30 by 30 nm. The TEM study combines bright field imaging and selected area electron diffraction (SAED) of pyrrhotite. Unfortunately the grains showed no perfect orientation perpendicular to the c-axis so the diffraction patterns could not be used for a polytype interpretation. However, the NiAs cell was observed at several places of the investigated grains indicating that the studied iron sulfide was actually pyrrhotite (Nakazawa and Morimoto 1971). Another difficulty is that vacancies tend to become disordered under the electron beam (Nakazawa et al. 1975; Pósfai et al. 2000), so it was very difficult to obtain diffraction patterns from the ion-milled samples.

RESULTS

Sulfide Petrography

In shale and slate-clasts of the upper part of the polymict lithic breccia unit, pyrrhotite appears as small (<10 μm) relics in pyrite, indicating a transition from pyrrhotite to pyrite. The sulfide assemblage consists of pyrite, pyrrhotite, and chalcopyrite, which have grown parallel and oblique to the cleavage affirming a genesis syn- and/or post-genetic to the Birimian metamorphism and deformation. Beside pyrite

Table 1. Curie temperatures (T_C) from heating runs, medium destructive field (MDF), coercive force (H_c), saturation remanence (M_r), and saturation magnetization (M_s) and field-dependence of magnetic susceptibility (χ_{hd}) for impact and target lithologies of the LB-07A and LB-08A drill core. H_c, M_R, and M_S and corresponding T_C are Helsinki data. Others are Heidelberg data. Lithologies are from Koeberl et al. (2007).

Depth (m)	Lithology	T_C1 (°C)	T_C2	T_C3	T_C4	MDF (mT)	H_c (mT)	M_r (mAm²/kg)	M_s (mAm²/kg)	M_r/M_s
LB-07A										
334.5	Polymict lithic breccia			500						
346.96	Polymict lithic breccia			476						
349.26[a]	Polymict lithic breccia	314	353	–		19				
349.5	Polymict lithic breccia	311		477			21	6.82	69.61	0.10
354.20	Polymict lithic breccia	310	–	445		48				
356.32	Polymict lithic breccia	313	–	–						
356.4	Polymict lithic breccia	314		474			30	13.34	27.01	0.49
360.35	Polymict lithic breccia	312	–	–		26				
360.35	Polymict lithic breccia	–	–	–						
368.9	Suevite	312		469			28	4.89	8.6	0.57
375.04	Polymict lithic breccia					30				
375.15	Polymict lithic breccia			491						
376.00	Polymict lithic breccia	312	–	–		27				
376.00	Polymict lithic breccia	–	–	–						
380.87	Suevite	–	–	–						
380.76	Suevite					20				
384.78	Suevite	313		515	635		28	17.2	34.76	0.49
385.41	Suevite					32				
389.73	Suevite	315	–	530		42				
390.13	Polymict lithic breccia	310	344	538						
400.48	Suevite	309		488			21	5.99	77.95	0.08
403.91	Suevite	310	–	–		63				
404.45	Suevite	310		556			34	8.65	22.36	0.39
408.59	Suevite	312	–	–		12				
410.21	Suevite	311	403	542			20	21.49	58.28	0.37
410.27	Suevite	–	330	–		35				
431.23	Suevite	314		503			34	7.37	15.93	0.46
438.90	Monomict lithic breccia	309	–	525						
442	Monomict lithic breccia	311		523	633		33	8.31	17.39	0.48
445.87	Monomict lithic breccia	315		571	631		17	3.08	88.31	0.03
471.88	Metapelite	305		511	613		36	11.13	18.1	0.61
482.1	Metapelite	310		510	616		29	77.59	153.3	0.51
539.97	Metapelite	311	–	–		45				
543.09	Metapelite	300	–	–						

[a]Further T_C at 155.

alteration, a replacement of elongated ilmenite laths by Fe sulfides and rutile was observed (Fig. 1c). In a first step, ilmenite is decomposed to pyrrhotite and rutile and in a second step, with increasing sulfur fugacities, pyrrhotite is decomposed to pyrite and rutile. Therefore changing redox conditions accompanied the rock history before the impact event. The alteration of pyrrhotite into pyrite and Fe oxides is restricted to the upper part of the drilled impact lithologies. Magnetite has not been observed microscopically confirming the rare observation of magnetite-related magnetic transition temperatures in κ-T curves (see below). In the impact breccias, pyrite is often strongly cataclased and pyrrhotite shows distinct fracturing (Fig. 1d). With increasing depth, pyrrhotite and rutile are the dominating opaque phases, but the inhomogeneously distributed pyrrhotite shows no obvious trend in abundance with depth. The amount of pyrrhotite is mostly below 1 vol%. In a sulfide vein within a greenschist clast in the polymict lithic breccia unit (376.0 m), pyrite, pyrrhotite, chalcopyrite, millerite [(Fe,Ni)S], and sulfoarsenide [(Fe,Ni,Co)AsS] occur (Fig. 1b). These minerals were also observed together with rare melt fragments in the polymict lithic breccia unit (Fig. 1a). The low amount and inhomogeneous distribution explain the absence of pyrrhotite-related Curie temperatures in some samples (Table 1) and the variation in magnetic susceptibility (see Fig. 7 and Elbra et al. 2007).

Table 1. *Continued*. Curie temperatures (T_C) from heating runs, medium destructive field (MDF), coercive force (H_c), saturation remanence (M_r), and saturation magnetization (M_s) and field-dependence of magnetic susceptibility (χ_{hd}) for impact and target lithologies of the LB-07A and LB-08A drill core. H_c, M_R, and M_S and corresponding T_C are Helsinki data. Others are Heidelberg data. Lithologies are from Koeberl et al. (2007).

Depth (m)	Lithology	T_C1 (°C)	T_C2	T_C3	T_C4	MDF (mT)	H_c (mT)	M_r (mAm²/kg)	M_s (mAm²/kg)	M_r/M_s
LB-08A										
255.45	Polymict lithic breccia	–	–	538		12				
271.41	Meta-graywacke	299	–	–						
271.77	Meta-graywacke	303	331	556						
278.71	Meta-graywacke	310	–	560		8				
285.32	Metapelite	312	–	–		15				
309.1	Meta-graywacke	320		522			28	9.13	23.85	0.38
313.38	Meta-graywacke	312		565	625		23	4.67	80.42	0.06
318.02	Metapelite	317		548	591		26	17.09	102	0.17
355.12	Meta-graywacke	315	353	465						
359.64	Metapelite	–	–	–		25				
359.98	Metapelite	312		523	608					
361.08	Meta-graywacke			541						
369.03	Meta-graywacke	313		532						
381.82	Metapelite	299					31	10.06	23.43	0.43
381.93	Metapelite	299		548			25	10.24	23.65	0.43
384.66	Metapelite	299		500			34	82.87	185.2	0.45
387.41	Metapelite	296		516			34	29.04	65.9	0.44
389.28	Meta-graywacke						32	1.23	2.42	0.51
392.54	Meta-graywacke	303		524			30	3.52	7.38	0.48
392.54	Meta-graywacke	319		506						
392.73	Meta-graywacke	311	–	–		16				
392.73	Meta-graywacke	316	–	–						
394.1	Meta-graywacke			492						
397.15	Meta-graywacke	301		539			25	5.29	13.99	0.38
397.15	Meta-graywacke	312		542						
400.2	Meta-graywacke	299								
427.63	Metapelite	310		563			33	14.4	29.32	0.49

Electron microprobe analyses of pyrrhotite revealed that the Fe content ranges from 44.8 to 47.9 atom% (Table 2). However, this large variation was only found in a shale-clast from 349.26 m (polymict breccia unit), while pyrrhotite in the matrix of the polymict lithic breccia from 354.2 m shows values between 45.6 and 46.9 atom%. The vein pyrrhotite in the greenschist from 376.0 m, which is associated with pyrite, chalcopyrite, millerite and Ni-Co-bearing sulfoarsenide, has Fe contents between 45.2 and 46.6 atom%. The latter also displays Ni contents up to 1.3 atom%, which is typical for pyrrhotite in mafic rocks associated with Ni-Co sulfides (e.g., Kontny et al. 2000). Co contents are always below 0.4 atom%. Most of our samples have a composition that is in accordance with the stability field of the ferrimagnetic 4C pyrrhotite type (46.4–46.9 atom%) (Kissin and Scott 1982) if the sum of Fe, Ni, and Co is considered. Only few analyses reveal a higher metal content indicative for antiferromagnetic types. The low metal contents in the shale-clast of 349.26 m (LB-07A) are interpreted as a result of oxidation of pyrrhotite, which can cause a distinct metal deficiency.

Table 2. Mineral chemical data in atom% of pyrrhotite (standard deviation is given in brackets; *n* is number of analyses).

Depth (m)	349.26	354.20	376.0
n	13	11	19
S	53.97 (0.83)	53.34 (0.40)	53.27 (0.14)
Fe	45.78 (0.84)	46.02 (0.41)	46.09 (0.43)
Ni	0.16 (0.08)	0.42 (0.26)	0.60 (0.32)
Co	0.05 (0.05)	0.15 (0.11)	0.02 (0.06)

Microstructures in Pyrrhotite

Shock metamorphic features like the occurrence of different PDFs in quartz and calcite, the observation of rare melt fragments, and the near-absence of diaplectic glass suggest peak shock pressures of less than 26 GPa for the BCDP impact lithologies (Deutsch et al. 2006, 2007). The strong brecciation of the target rocks (Fig. 1a) can be interpreted as a sign for high differential stresses under relatively low temperatures during the impact event.

Coating the polished sections with ferrofluid, which sticks to magnetic phases (see, e.g., Kontny et al. 2000), revealed that the ferrimagnetic pyrrhotite dominates, but sometimes two different types, the antiferromagnetic hexagonal and the ferrimagnetic monoclinic type, occur. Both types can be easily distinguished microscopically because the ferrofluid only sticks to the latter one. In these cases, the ferrimagnetic type occurs at the rim and the antiferromagnetic one in the core indicating a replacement of the latter (Fig. 1e). Although pyrrhotite grains are mostly not as strongly brecciated as pyrite grains, a distinct fracturing (Fig. 1d) and grain reduction can be observed throughout the drilled depth interval. Microstructures in pyrrhotite cannot be further studied by optical microscopy, although a patchy and streaky distribution of ferrofluid was observed in some areas (Figs. 1d and 1e), indicative for the characteristic twinning of monoclinic 4C pyrrhotite (e.g., Pósfai et al. 2000). Larger pyrrhotite aggregates are polycrystalline and the ferrofluid streaks show different orientations (Fig. 1f).

Pyrrhotite occurs in small amounts (mostly less than 1–2 vol%) together with pyrite in the impact breccia. Therefore it was not easy to find appropriate grains for TEM investigation. The energy dispersive spectrum of the investigated sulfide grain from the polymict impact breccia of 354.2 m presented in the inlay of Fig. 2b shows only Fe and S in a ratio close to unity, which is indicative for pyrrhotite.

Bright-field TEM images of pyrrhotite often show twin boundaries as it is shown in Fig. 2a. Twinning in pyrrhotite is typical for the ordered 4C superstructure, but has not been observed for the other pyrrhotite modifications (Pósfai et al. 2000; Sharp and Kontny, unpublished data). From a study on metamorphic pyrrhotite of the KTB drilling, Germany, we know that twin lamellae can occur in variable sizes from 50 to several hundred nanometers (Kontny et al. 2000; Pósfai et al. 2000).

In the polymict impact breccia from the Bosumtwi drilling, the twin lamellae of pyrrhotite show strong brittle to brittle-ductile deformation features like planar defect structures (Fig. 2b), kink-bands (Fig. 2c), and bended twin lamellae (Fig. 2d). The planar defect structures resemble PDFs in quartz (see, e.g., Morrow 2006; Trepmann and Spray 2006) and we interpret these features as a result of shock metamorphism. The bending of twin lamellae and the kink-bands indicate shock-wave associated differential strain at low temperatures. Parallel planar deformation structures have formed by compression probably during the impact event perpendicular to bended and slightly kinked twin lamellae, while open voids filled with undeformed, secondary quartz have been formed after decompression in the same direction (Fig. 2d).

Magnetic Mineralogy from χ-T Curves

Curie temperatures (T_C) were determined from temperature-dependent measurements of the magnetic susceptibility (χ-T curves) (Fig. 3) and are presented in Table 1. Rock magnetic properties in all lithologies are carried mainly by pyrrhotite (T_C: 310–320 °C). In most samples, minor amounts of phases with T_Cs between 450 and 590 °C occur in the heating run. Some χ-T curves have T_Cs higher than 600 °C, which is typical for a hematite-like phase. A Verwey transition around –150 °C, which indicates that magnetite has been in the rock before heating, has been observed only in one meta-graywacke sample (LB-08A, 271.41 m) (Fig. 3f). The absence of the Verwey transition in all other samples indicates that magnetite either has been formed during the heating experiment or occurs in very minor amounts in single domain grain size (e.g., Muxworthy 1999) as is indicated in Fig. 3e for a sample from the uppermost part of drill core LB-08A. Further T_Cs at ~155 °C and ~330–350 °C occur in some samples (Figs. 3a and 3c). A T_C at ~155 °C could indicate some very minor amounts of a substituted magnetite or chromite, which is in agreement with minor mafic target rocks. But the irreversibility of this phase (it no longer occurs in the cooling curve) implies a metastable behavior upon heating, which is not in agreement with a stoichiometric substituted magnetite or chromite. More likely are metastable Fe hydroxides. Nickel with a T_C of 358 °C (Hunt et al. 1995), greigite (Fe_3S_4) with a T_C of 333 °C (Hunt et al. 1995) or ~350 °C (Dekkers 1997) as well as anomalous pyrrhotite with a T_C at about 350 °C (e.g., Rochette et al. 1990) can be considered as possible candidates for the T_C between 330 and 350 °C. As this phase is not reversible during heating, nickel can be excluded as an explanation and the Fe sulfides are the more likely candidates. Oxidation of pyrrhotite (see above and compare sample 349.26 m in Table 2) results in lower metal content and might be in line with metastable Fe sulfides like ferrimagnetic smythite (Fe_9S_{11}) or greigite (Fe_3S_4). While the latter one is only typical for sedimentary and not for metamorphic environments, smythite seems to be the more probable candidate (see also Jover et al. 1989).

Magnetic phases other than pyrrhotite have not been identified microscopically using the ferrofluid method (see above). Furthermore, few samples show a purely paramagnetic behavior (see Table 1, e.g., at 380.87 m) confirming the optical observation of an inhomogeneous distribution of pyrrhotite.

In most samples heated up to 700 °C, irreversible behavior has been observed with formation of magnetite or a magnetite-near phase with T_Cs between 445 and 605 °C (Fig. 3). Only few samples, which do not contain pyrrhotite but minor amounts of very small-grained magnetite (Fig. 3e), have a reversible χ-T curve. This is a typical behavior for pure stoichiometric magnetite. In all other samples heated up to 700 °C, magnetite formation is affirmed by the Verwey transition at about –150 °C in a second cooling run (Figs. 3g and 3h). T_Cs higher than 590 °C probably indicate maghemitization of magnetite during further heating. Pure magnetite can be produced during heating of pyrrhotite (e.g.,

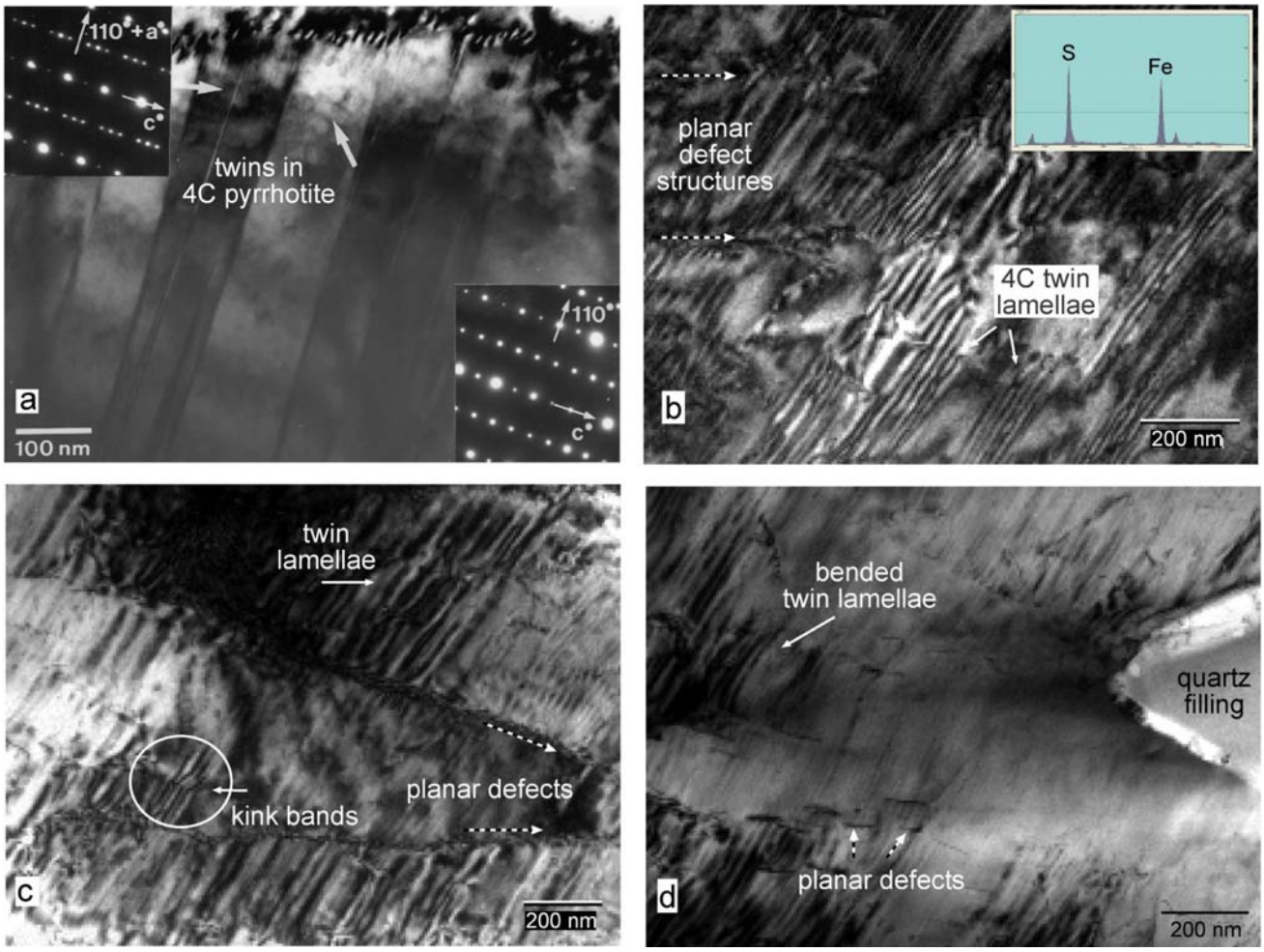

Fig. 2. Bright-field TEM images of typical features of pyrrhotite from metamorphic and impact rocks. a) Twinned 4C pyrrhotite with twin boundaries subparallel to (001) plane. SAED in upper left corner shows both twin orientations c*-a* and c*-110* for the dark twin lamella, which contains small nm sized twin lamella (white arrow). SAED in lower right corner shows c*-110* orientation for the bright twin lamella (white arrow). Sample is from paragneiss with metamorphic pyrrhotite from 564 m of the KTB drilling, Germany (photo by T. Sharp, Arizona). b) Patches of twinned pyrrhotite are separated from areas without visible twinning by parallel planar defect structures perpendicular to twin lamellae. Inlay shows the energy dispersive spectrum of the pyrrhotite investigated in detail by EDX with Fe and S in a ratio near unity. c) Planar defect structures lying perpendicular to a strongly twinned pyrrhotite. Note the kink-band in lower left area. d) Parallel deformation features perpendicular to bended and slightly kinked twin lamellae and open void filled with undeformed, secondary quartz. b–d) Polymict lithic breccia from 354.2 m (see also Fig. 1a).

Dekkers et al. 2000), but not from nickel. During the cooling run, additional T_Cs between 420 and 500 °C probably indicate the formation of an intermediate ferrimagnetic spinel phase during the heating experiment. Spinel phases can be produced by heating of Mg-Fe-bearing carbonates (e.g., Ellwood et al. 1989; Just 2005), which were mainly observed in breccias. Small amounts of magnetite can also be formed by heating of fine-grained clay minerals in argon atmosphere above 600 °C as reported by Just (2005). Clay minerals and carbonates were identified by XRD (see above).

Samples that were only heated up to 400 °C showed a very good reversibility of pyrrhotite TC (Fig. 3c). Therefore, the reaction of pyrrhotite to magnetite occurs above 400 °C as already documented (e.g., Kontny et al. 2000).

Demagnetization Behavior

Thermal demagnetization of the samples confirmed that the NRM is removed by thermal demagnetization up to 340 °C (Fig. 4). This means that the remanence is mainly carried by pyrrhotite, similar to what is described for the Lappajärvi impact structure, Finland (Pesonen et al. 1992). In samples from the uppermost part of the drill core LB-08A, pyrrhotite is a minor component and the weak magnetization is mainly carried by a magnetite-like phase (Fig. 4d). Stable paleofield directions are also mainly carried by pyrrhotite and, in surface-near samples, additionally by magnetite. Mostly, only one shallow normal stable paleofield direction besides a viscous component was observed, which is

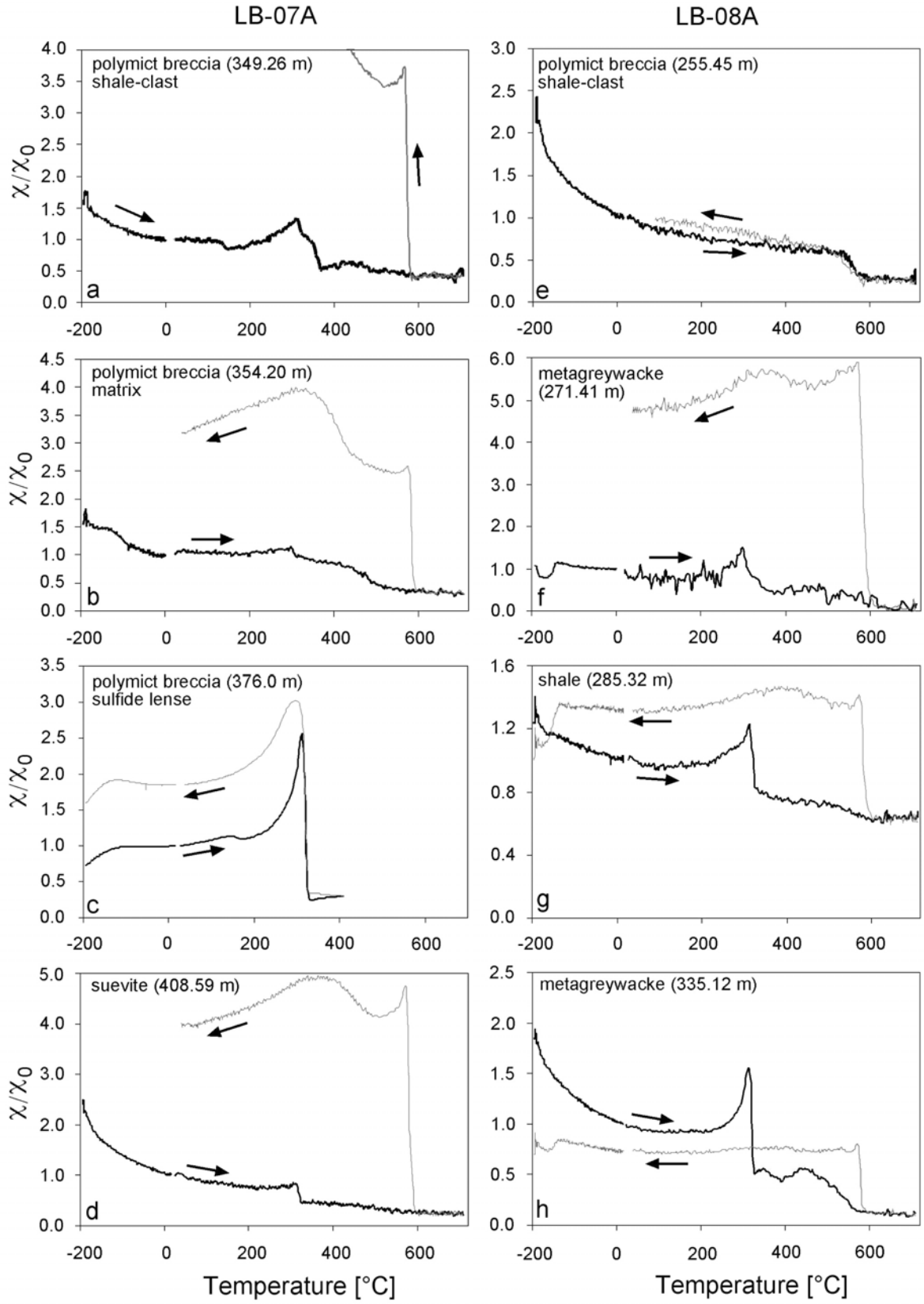

Fig. 3. Normalized susceptibility as function of temperature between –192 and 700 °C. Black line is the heating curve; gray line is the cooling curve (also indicated by arrows). Curie temperatures are summarized in Table 1.

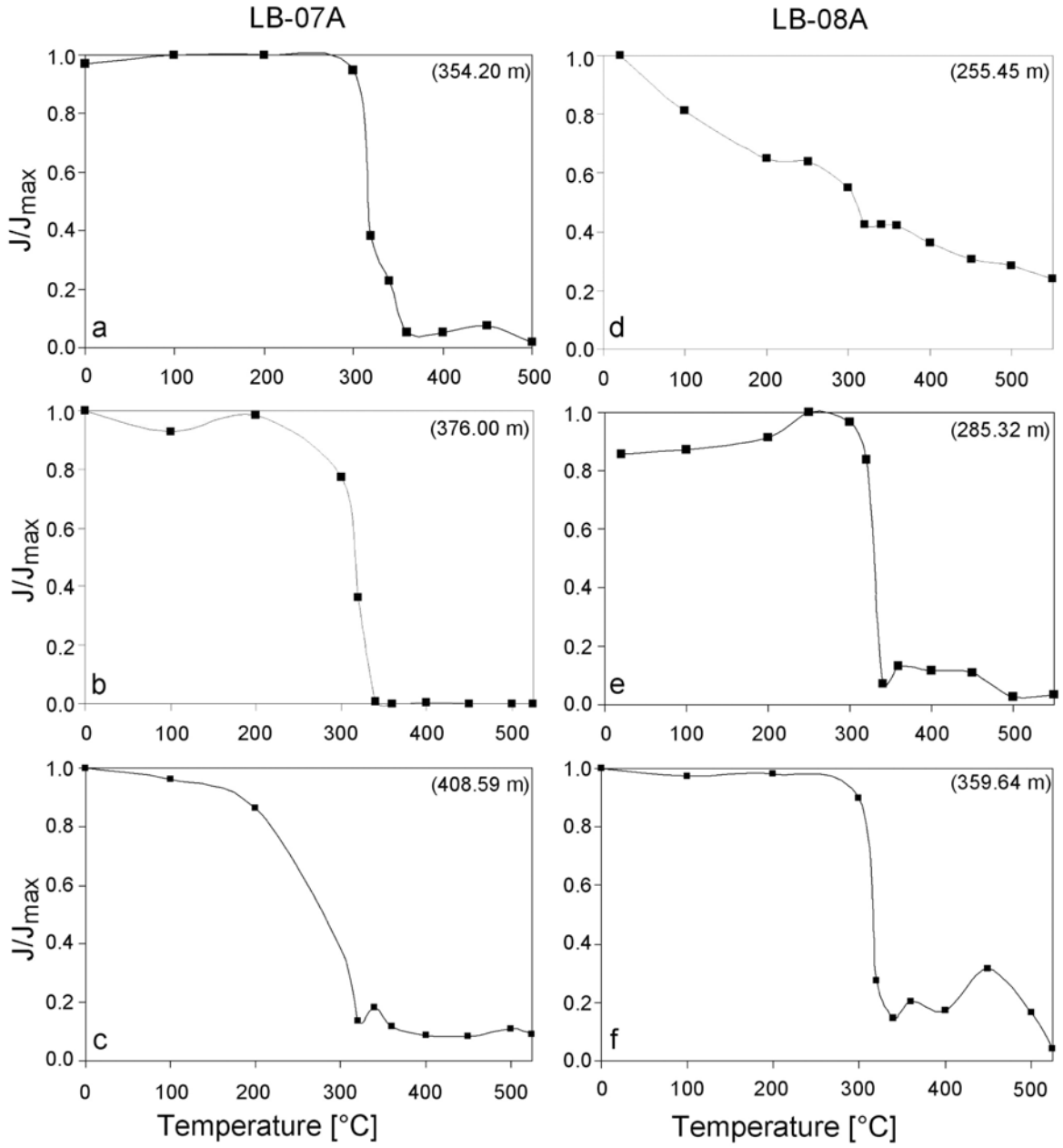

Fig. 4. Intensity decay of the NRM during thermal demagnetization for different depths and lithologies of the LB-07A and LB-08A. a), b), and d) Polymict lithic breccia units. c) Suevite. e) Shale. f) Phyllite.

interpreted as the Lower Jaramillo N-polarity chron. (Elbra et al. 2007). Therefore, the occurrence of magnetite (Figs. 3e and 4d) is related to near subsurface alteration and is interpreted to be a pre-impact feature.

During AF demagnetization the pyrrhotite-bearing samples showed variations in their magnetic hardness, which we determined from the medium destructive field (MDF) (Figs. 5a and 5c) and hysteresis measurements (Table 1). The MDF is the field that is required to reduce remanence to one-half its initial value and is a measure of the bulk coercivity. MDF values range between 8 and 63 mT (Table 1). The lower values are mainly found in rocks from drill core LB-08A, either where a magnetite-near phase was observed by χ-T curves or where meta-graywackes occur. The breccia lithologies mostly show the higher MDF values, in accordance with a smaller grain size. Coercive forces (H_C) from hysteresis measurements (Fig. 6; Table 1) range between 8 and 35 mT, similar to the values obtained from the MDF. Most values from both types of measurements vary between 20 and 35 mT and are in very good agreement with each other. The M_r /M_s ratio shows an average of 0.44 for 31 samples from LB-07A and LB-08A (Table 1). This is in good

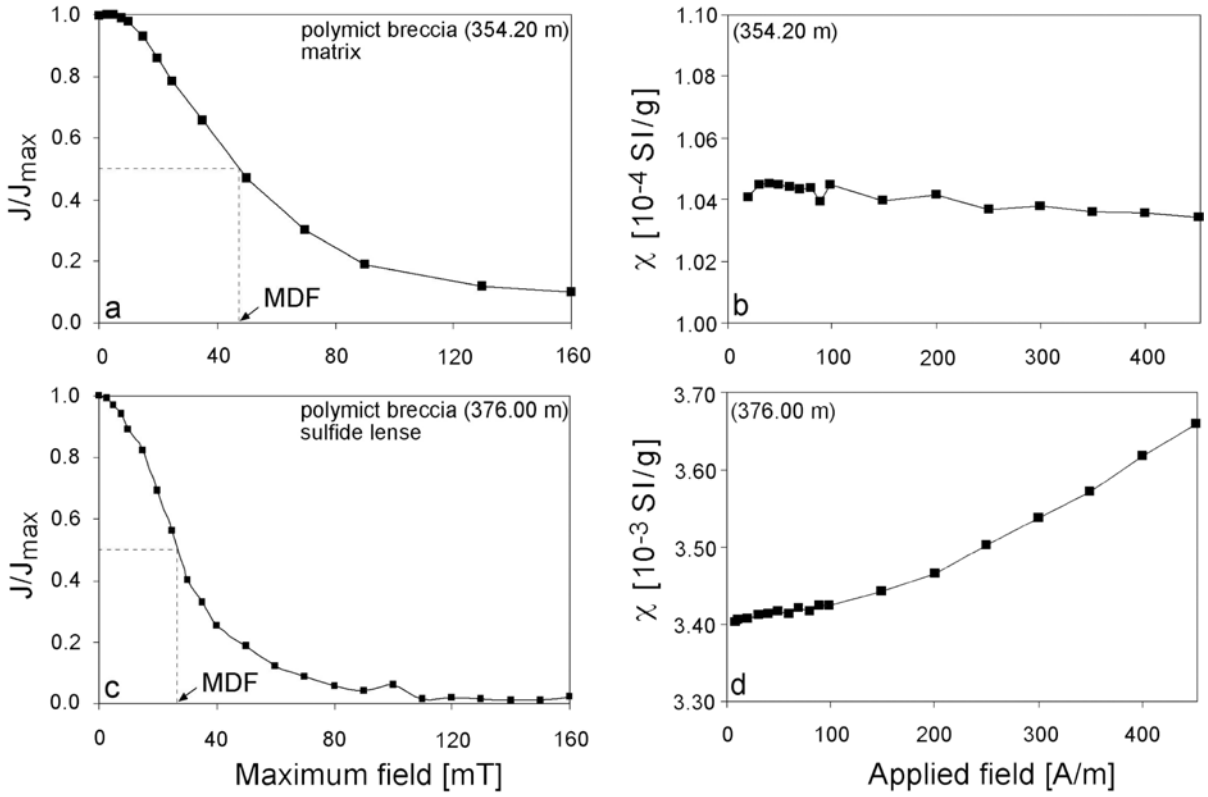

Fig. 5. Alternating field demagnetization of NRM and field-dependence of magnetic susceptibility for the polymict breccia at 354.20 m depth showing high MDF (a) and no field-dependence (b), and for the sulfide lens in the greenschist clast at 376.0 m depth with a lower MDF (c) and a strong field-dependence (d).

agreement with the hysteresis loops of a Devonian diabase containing pyrrhotite as main magnetic mineral with a wide range of grain size, from <1 to >100 m (Soffel 1981) and M_r/M_s ratio of about 0.5. The coercive force in the study by Soffel (1981) was 18 mT. The higher coercive forces found in our study is in line with a higher amount of smaller magnetic grain sizes, which increase magnetic hardness. Higher coercive forces (26–46 mT) are also described for the Lappajärvi impact structure, where also pyrrhotite is described as magnetic carrier of NRM in the impact lithologies (Pesonen et al. 1992).

Small magnetic grain sizes of pyrrhotite are magnetically also confirmed by the absence of the field-dependence of magnetic susceptibility in most samples (see χHd in Table 3 and Fig. 5b). Few exceptions occur, which show a distinct field dependency (Fig. 5d). Worm et al. (1993) have shown that the susceptibility of pyrrhotite and its field dependence strongly increase with grain size. While the susceptibility of grains smaller than 30 μm is field independent it increases for millimeter-size crystals in fields of about >10 A/m. This observation suggests that the magnetically effective grain sizes in our study are mostly below the 30 μm threshold, which strengthens the significance of microstructures within the pyrrhotite grains for its rock magnetic properties.

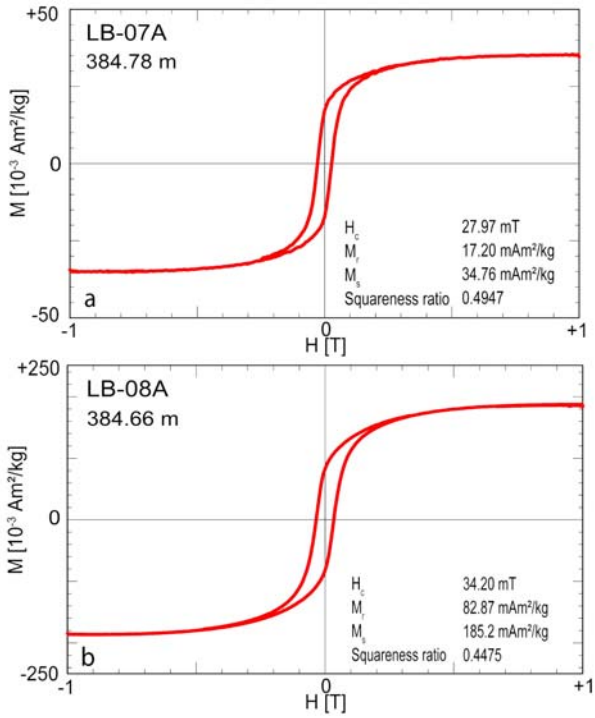

Fig. 6. Normalized hysteresis loops with paramagnetic correction at room temperature for a) suevite at 384.78 m and b) shale at 384.66 m.

DISCUSSION

Rock Magnetic Data for Magnetic Modeling

Magnetic susceptibility (χ), natural remanent magnetization (NRM), and Koenigsberger ratio ($Q = M_{rem}/\chi \times M_{ind}$) of impact lithologies and target rocks from LB-07A and LB-08A are shown in Table 3 and Figs. 7a and 7b, in comparison to the data from the surrounding suevite samples of Plado et al. (2000) and our own measurements on surface samples. In the drill core of LB-08A, NRM and Q-ratio show a distinct increase from 230 to 260 m (see Elbra et al. 2007). This increase can be correlated with the onset of pyrrhotite in the rocks. Values for magnetic susceptibility (108–10.630 × 10^{-6} SI), NRM (0.2 mA/m–43 A/m), and Q-ratio (0.03–250) show a large range, depending on the amount of pyrrhotite in the sample and probably also on the degree of shock effects. Sixty-three percent of the drill-core samples show Q values >1 and 21% >10. Fifty-six percent of the NRM values are >0.01 A/m and 23% >0.1 A/m. In general, magnetic susceptibility and NRM correlate positively, with largest values up to 10×10^{-3} SI units and up to 43 A/m, respectively, in sample 376.00 m from a pyrrhotite-bearing sulfide lens in a greenschist clast. Polymict lithic breccias show χ values mostly below 0.8×10^{-3} SI and NRM intensities between 0.4 and 200 mA/m, similar to the majority of the metasedimentary target rocks. Therefore, no significant difference was found for these rock magnetic parameters between the basement rocks and impact breccia. However all values, especially for the basement rocks, are distinctly higher than the one reported by Plado et al. (2000) for surrounding rocks of Lake Bosumtwi (Fig. 7) and for the model used by Plado et al. (2000). Only the polymict lithic breccias from above about 260 m of LB-08A, where no or only minor pyrrhotite occur, are similar to the surface samples.

The majority of the investigated samples from LB-07A and LB-08A drill cores have Q values above 1 indicating that the remanent magnetization dominates over the induced magnetization (Fig. 7b; see also Plado et al. 2000). Magnetic susceptibility as function of temperature and thermal demagnetization of NRM revealed that pyrrhotite is the main carrier of magnetization. Additionally, two or three further magnetic phases (probably smythite/anomalous pyrrhotite, magnetite-like phase, rare hematite) were identified but they do not carry a significant remanence, unless in the uppermost samples of drill core LB-08A where magnetite and few pyrrhotite occur together. Although the samples from the upper part of LB-08A carry a very low magnetization, the direction is quite stable, and both relics of pyrrhotite and magnetite seem to be remagnetized (compare Fig. 6 of Elbra et al. 2007). This implies that the surface-near alteration of pyrrhotite already took place before the impact event. From the KTB drilling in Germany it is well known that in paragneisses pyrrhotite is altered into pyrite down to a depth of about 200 m (Kontny et al. 1997) and start to occur below that depth. The oxidation of pyrrhotite into pyrite and a few magnetite is not unusual and has been observed in several Paleozoic rocks from the European Variscides creating magnetic anomalies (e.g., Franken et al. 1985; Pucher 1994).

Modeling of the magnetic field of the Bosumtwi impact structure requires a much stronger magnetization than those measured for the impactites from surface exposures around the lake and even those of the drill cores reported in this study (Ugalde et al. 2007b; Plado et al. 2000) (Fig. 7). Surprisingly, the supposed high content of melt rocks was not observed in the drill core LB-08A but Coney et al. (2006) reported 0.5–36 vol% impact-melt particles in the suevites of drill core LB-07A. Nevertheless, we suspect from our observations that TRM acquired due to extensive rock melting is unlikely, although pyrrhotite formed from melt was rarely observed (Fig. 8).

Magnetization Mechanism for Pyrrhotite

Prominent magnetic anomalies over large impact craters are attributed to remanent magnetization and often are characterized by (extremely) high Koenigsberger values (e.g., Pilkington and Grieve 1992). One outstanding example is the very large Vredefort impact structure, South Africa, where the magnetic anomaly near the center is also attributed to remanent magnetization with Q values ranging between 1.3 and 186 (Hart et al. 1995). For the Bosumtwi drill cores, locally similar high values were measured (Table 3). The target rocks at Vredefort are magnetite-bearing Archean granite-gneisses but the accessory magnetite (aggregates several hundredths of μm large, mostly below 2 vol%) is neither sufficient in concentration nor can explain the extremely high remanent magnetization up to 130 A/m (Hart et al. 1995). Petrographic observations including electron and magnetic force microscopy revealed additionally to the large magnetite grains <5 μm size magnetite particles with high aspect ratios (15:1) along PDFs of quartz. This magnetite crystallized from locally formed micromelts that intruded along zones of weakness such as microfractures and PDFs shortly after the shock event (Cloete et al. 1999). High remanences in the Vredefort basement is related to high frequencies of microdeformation phenomena, in particular PDFs in quartz. The ultrafine-grained magnetite along shock-induced PDFs behave as single domain grains. According to Kletetschka et al. (2000, 2004), single domain magnetite has a ten times higher potential to acquire a TRM compared to multidomain magnetite. Therefore, such microstructural features are able to explain high remanences in impact rocks, such as in the Vredefort case. Shock experiments between 4.5 and 35 GPa on a “titanomagnetite”-bearing diabase revealed no microstructural shock effect in “titanomagnetite” but a tiny intergrowth of magnetite, ilmenite, and titanite (Langenhorst et al. 1999), which seem to explain the unusual shock hardening (Pesonen et al. 1997).

Table 3. Rock magnetic properties of impact and target lithologies of the LB-07A and LB-08A drill cores. *n* = number of specimen, χ = magnetic susceptibility measured at 300 A/m, χHd = field dependence parameter, NRM = natural remanent magnetization, and Q value = Koenigsberg ratio. Lithologies are from Koeberl et al. (2007).

Depth (m)	Lithology	Remarks[a]	*n*	$\chi_{300\ A/M}$ (10^{-6} SI)	χHd	NRM (A/m)	Q value[b]
LB-07A							
347.19	Polymict lithic breccia	Shale-clast	1	807	2.9	1.34E-01	6.53
349.26	Polymict lithic breccia	Shale-clast	5	683		8.16E-01	47.88
354.20	Polymict lithic breccia	Cd, matrix supported	3	256	–0.3	2.72E-02	4.18
355.71	Polymict lithic breccia	Cd, matrix supported	2	324	–0.3	5.21E-02	6.31
356.32	Polymict lithic breccia	Md, fine-grained	4	108	–1.4	1.35E-03	0.55
360.35	Suevite	Cd, matrix-supported	4	419		7.90E-02	10.52
375.04	Polymict lithic breccia	Md	4	868	11.6	1.03E+00	47.78
376.00	Polymict lithic breccia	Md, greenish	4	10,630	2.9	4.30E+01	100.48
378.30	Polymict lithic breccia	Md, greenish	7	213		2.28E-03	0.43
380.87	Suevite	Md, greenish	5	195	0	1.24E-02	2.31
380.76	Suevite	Cd	12	227	5.5	2.90E-02	3.16
384.74	Suevite	Cd	3	406	3.9	3.33E-02	3.24
385.41	Suevite	Md, gray	3	263		2.83E-02	5.44
389.73	Suevite	Shale	6	1033	–0.3	6.65E+00	251.99
390.13	Polymict lithic breccia	Cd	1	943	–0.5	1.62E+00	67.59
398.17	Suevite	Md	1	330	–1.1	8.10E-02	9.65
400.98	Suevite	Cd	1	369	0	7.56E-03	0.80
402.71	Suevite	Cd	2	497	–0.7	4.05E-02	3.22
403.61	Suevite	Cd	4	146	0.5	3.47E-03	0.92
403.91	Suevite	Md	3	326	0.1	3.96E-02	4.77
408.09	Suevite	Cd, polymict	1	494	0.3	1.18E-01	9.37
408.33	Suevite	Cd	4	504		1.48E-02	1.84
408.59	Suevite	Cd	3	220	0.1	9.28E-03	1.62
409.97	Suevite	Cd	1	512	–0.7	4.80E-02	3.68
438.90	Monomict lithic breccia	Md	2	290	0	2.19E-02	2.69
470.32	Metapelite	Cd	1	386	0	1.77E-01	18.01
539.97	Metapelite	Cd	4	303	0.3	5.52E-02	7.31
LB-08A							
236.03	Polymict lithic breccia	Shale	4	336	–1.6	2.38E-04	0.03
238.95	Suevite	Cd, polymict	2	259	–0.8	7.81E-03	1.18
239.36	Polymict lithic breccia	Cd, polymict	2	213	0.2	2.83E-04	0.05
241.70	Polymict lithic breccia	Shale	1	330	–0.3	5.18E-04	0.06
255.45	Polymict lithic breccia	Shale	4	108		8.92E-04	0.31
258.28	Polymict lithic breccia	Cd	9	214		8.09E-03	1.51
258.74	Polymict lithic breccia	Cd	4	826	0.13	5.33E-03	0.46
271.41	Meta-graywacke		4	125	1.8	5.91E-03	1.76
271.77	Meta-graywacke		4	293		8.70E-03	1.11
274.37	Meta-graywacke		2	205	–0.1	6.87E-04	0.04
278.71	Meta-graywacke	Fine-grained	4	521		7.95E-02	6.05
283.20	Meta-graywacke	Fine-grained	2	287	–0.8	9.60E-04	0.13
285.32	Metapelite	Shale	5	273		8.05E-02	14.56
297.39	Meta-graywacke	Fine-grained	2	330	0.19	1.97E-01	23.48
303.51	Meta-graywacke	Fine-grained	4	236		8.85E-02	14.94
304.76	Meta-graywacke	Shale	1	205			
319.96	Metapelite	Phyllite	1	188	1.2	3.21E-04	0.07
355.12	Meta-graywacke	Phyllite	2	526	0.7	1.24E-01	9.31
356.97	Meta-graywacke	Fine-grained	1	239	–1.6	1.59E-03	0.26
359.64	Metapelite	Phyllite	4	314		2.01E-02	2.52
392.73	Meta-graywacke	Foliated	5	316	–0.3	1.82E-02	2.27
435.39	Meta-graywacke	Fine-grained	2	276	0.2	9.79E-03	1.47
447.44	Meta-graywacke		1	330	–0.2	3.58E-04	0.04

[a]Cd = clast dominated; md = matrix dominated.
[b]Ambient field for calculation of Q was 32,000 nT.

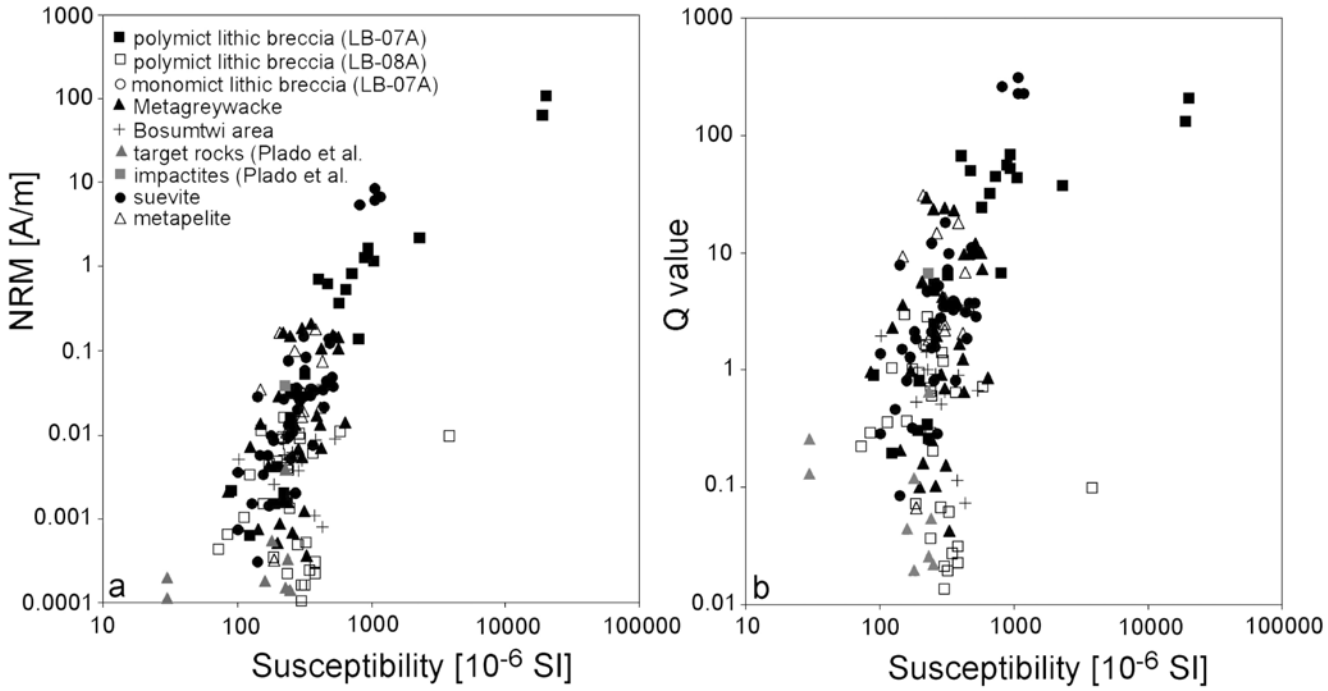

Fig. 7. Natural remanent magnetization (NRM) versus (a) susceptibility and (b) Koenigsberg (Q) ratio versus susceptibility for different impact and target lithologies of the BCDP drill cores and samples from the surface. Bosumtwi area denote different suevites and target lithologies from the surrounding of the crater (kindly provided by A. Deutsch, Münster.)

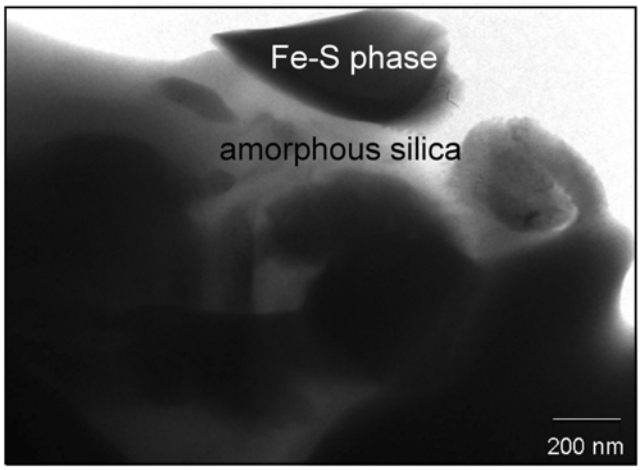

Fig. 8. TEM–bright field image showing Fe sulfide particle (most likely pyrrhotite) in amorphous silica. Polymict lithic breccia from 354.2 m of LB-07A drill core.

Pyrrhotite, formed from melt similar to that observed for magnetite in the Vredefort impactites, has also been observed in the LB-07A drill core (Fig. 8) but is of only minor significance. Furthermore, from our investigation it is not yet clear if the observed Fe sulfide actually is the ferrimagnetic pyrrhotite variety. Nonmagnetic modifications do not contribute to the rock magnetic properties.

Petrographic features documented in the Bosumtwi drill cores of this study allocate a pre-impact formation of pyrrhotite. The most prominent feature is a distinct fracturing and grain size reduction due to shock-induced brecciation, which can be observed throughout the drilled depth interval in the breccia units (Fig. 1).

Microscopic grain sizes show a large variation between a few micrometers and more than 500 μm. Therefore, the lack of field-dependence of magnetic susceptibility in many of our samples (Fig. 5; Table 3) was suspicious. We assume that domain wall movement during susceptibility measurements in different fields is inhibited by the observed microstructures like bending and kinking of twin lamellae, and parallel planar defect structures (Fig. 2). Furthermore, the defects seem to subdivide the ferrimagnetic domains and, probably, the shock pressure also destroys the ferrimagnetic ordering, giving rise to the formation of disordered pyrrhotite polytypes (e.g., Kissin and Scott 1982).

Our observations suggest that high differential strain during the shock event caused fracturing of pyrrhotite grains and microstructures in a submicron range, which are responsible for a significant reduction of effective magnetic grain size and thus magnetic hardening of pyrrhotite. Contemporaneously, the shock demagnetized the pyrrhotite. According to neutron diffraction studies under pressures at room temperature (Rochette et al. 2003), pyrrhotite undergoes a shock-induced ferrimagnetic to paramagnetic transition above about 2.8 GPa. For the BCDP drill cores, a maximum shock pressure of 26 GPa is derived from quartz deformation features (Deutsch et al. 2007), which implies a

demagnetization of the original remanence. Such an interpretation is also inferred for pyrrhotite-bearing shocked SNC meteorites, which are asserted to carry no pre-shock magnetic memory (Rochette et al. 2005). After the shock event, pyrrhotite acquired a stable remanent magnetization as proofed by paleomagnetic investigations (Elbra et al. 2007).

From deformation experiments it is known that pyrrhotite show a remarkable drop in strength in the temperature range between 200 and 300 °C (see Figs. 4 and 7 in Clark and Kelly 1973). While the temperature range between 200 and 300 °C is characterized by intense kinking, deformation twins dominate above 300 °C. In pyrrhotite from the Bosumtwi impact breccia, kink bands as well as planar features but no deformation lamellae were observed using optical and electron microscopy. The observed twin lamellae shown in Fig. 2 are clearly related to the ferrimagnetic pyrrhotite modification (see also Pósfai et al. 2000) and not to deformation. Therefore the deformation temperatures for the Bosumtwi pyrrhotite were most likely below 250 °C. Because temperatures were not above the Curie temperature of ferrimagnetic pyrrhotite (310 °C), the nature of the stable remanent magnetization is suggested to be not a TRM but seems to be some sort of shock-induced remanent magnetization (SRM) or partial thermoremanent magnetization (pTRM). According to data given by Clark (1983; see also data compilation in Kletetschka et al. 2000, 2004), single-domain pyrrhotite acquires a ten times higher remanence in small magnetic fields than multidomain pyrrhotite and a nearly equal high one than single-domain magnetite. The data from this study suggest that pyrrhotite acquired a stable remanent magnetization during shock-induced grain size reduction below its T_C. If also magnetite is remagnetized as indicated in this and the study of Plado et al. (2000), one would assume higher remagnetization temperatures. However, the very short time that was needed for this process (minutes to days) probably allows much lower remagnetization temperatures as it is indicated in the study of Dunlop et al. (2000).

CONCLUSIONS

The present survey on rock magnetic properties and magnetic mineralogy of the Bosumtwi drill cores LB-07A and LB-08A revealed ferrimagnetic pyrrhotite as the most important carrier of the remanent magnetization. The rocks reveal relatively high Q and NRM values compared to relatively low magnetic susceptibility (Fig. 7; Table 3). The low susceptibility is in accordance with the low amount of pyrrhotite (mostly below 1 vol%) in most of the samples. Microscopically, no other magnetic phase has been identified. But thermomagnetic curves revealed further magnetic phases (probably Fe oxide/hydroxide, anomalous pyrrhotite, magnetite, hematite), which are interpreted as alteration products of the sulfides, either before or after the impact event. In the surface samples and few samples of LB-08A, a magnetite phase carries the same (stable) paleofield direction as pyrrhotite (see also Elbra et al. 2007) affirming a pre-impact alteration. Although the grain sizes of pyrrhotite show a large variation, the numerous stress-induced nanostructures are assumed to behave as single-domain grains, which carry the stable and, compared to the amount of pyrrhotite, relatively high remanence. We suggest that the drilled rocks lost their pre-shock remanence memory during the shock event and acquired a stable magnetization during shock-induced grain size reduction below about 250 °C, which is clearly below the T_C of pyrrhotite (310 °C). The acquired remanence is therefore no TRM or CRM but some sort of SRM.

Although the volume of pyrrhotite in the rocks is very small (mostly below 1 vol%), the magnetization of the pyrrhotite-bearing impact lithologies is locally several times higher compared to the surrounding fall-out suevite (see Fig. 7). The surprising observations from the drill cores have not confirmed previous analyses of the airborne magnetic data (Plado et al. 2000) and numerical simulation (Artemieva et al. 2004), predicting a strong magnetic impact melt body underneath Lake Bosumtwi. From a new model considering marine magnetic data, the BCDP borehole and drill core petrophysics, and the mapped geology, it is concluded that there is no need for highly magnetic melt sheets (Ugalde et al. 2007b). These authors suggest that the granodiorites from the Kumasi batholith located northeast of the lake can cause the magnetic anomaly. However, no rock magnetic data are available at the moment to proof this interpretation and it remains an open question if not the remagnetization mechanism proposed in this study contributes significantly to the observed anomaly pattern.

Acknowledgments–Drilling at Bosumtwi was supported by the ICDP, the U.S. NSF-Earth System History Program under grant no. ATM-0402010, Austrian FWF (project P17194-N10), the Austrian Academy of Sciences, and by the Canadian NSERC. Drilling operations were performed by DOSECC. Our research was supported by the German Research Foundation under grant no. KO1514/2. We thank Carsten Vahle for discussions and Sandra Panienka for help in the magnetic laboratory at Heidelberg. Hans-Peter Meyer from the Mineralogical Institute, Heidelberg, is thanked for his help with electron microprobe analyses. Electron Microscopy was carried out at the EMAL of the University of Michigan (Ann Arbor, USA) during a research visit by A. K. Special thanks to EMAL's Carl Henderson for discussions and help and to Ben van der Pluijm for hosting the visit. P. Rochette, C. Carvallo, and B. Milkereit helped us to improve the original manuscript.

Editorial Handling—Dr. Bernd Milkereit

REFERENCES

Artemieva N., Karp T., and Milkereit B. 2004. Investigating the Lake Bosumtwi impact structure: Insight from numerical modeling. *Geochemistry Geophysics Geosystems* 5:1–20.

Boamah D. and Koeberl C. 2003. Geology and geochemistry of shallow drill cores from the Bosumtwi impact structure, Ghana. *Meteoritics & Planetary Science* 38:1137–1159.

Clark B. R. and Kelly W. C. 1973. Sulfide deformation studies: I. Experimental deformation of pyrrhotite and sphalerite to 2,000 bars and 500 °C. *Economic Geology* 68:332–352.

Clark D. A. 1983. Comments on magnetic petrophysics. *Exploring Geophysics* 14:49–62.

Cloete M., Hart R. J., Schmid H. K., Drury M., Demanet C. M., and Sankar K. V. 1999. Characterization of magnetite particles in shocked quartz by means of electron- and magnetic-force microscopy: Vredefort, South Africa. *Contributions to Mineralogy and Petrology* 137:232–245.

Coney L., Reimold W. U., Koeberl C., and Gibson R. L. 2006. Mineralogical and geochemical investigations of impact breccias in the ICDP borehole LB-07A, Bosumtwi impact structure, Ghana (abstract #1279). 37th Lunar and Planetary Science Conference. CD-ROM.

Deutsch A., Heinrich V., and Luetke S. 2006. The Lake Bosumtwi Crater Drilling Project (BCDP): Lithological profile of wellhole BCDP-8A (abstract #1292). 37th Lunar and Planetary Science Conference. CD-ROM.

De Wall H. 2000. The field-dependence of AC susceptibility in titanomagnetites: Implications for the anisotropy of magnetic susceptibility. *Geophysical Research Letters* 27:2409–2411.

Dekkers M. J. 1997. Environmental magnetism: An introduction. *Geologie en Mijnbouw* 76:163–182.

Dekkers M. J., Passier H. F., and Schoonen M. A. A. 2000. Magnetic properties of hydrothermally synthesized greigite (Fe_3S_4)—II. High- and low-temperature characteristics. *Geophysical Journal International* 141:809–819.

Deutsch A., Luetke S., and Heinrich V. 2007. The ICDP Lake Bosumtwi impact crater scientific drilling project (Ghana): Core LB-08A litho-log, related ejecta, and shock recovery experiments. *Meteoritics & Planetary Science* 42. This issue.

Dunlop D. J., Özdemir Ö., Clark D. A., and Schmidt P. W. 2000. Time-temperature relations for the remagnetization of pyrrhotite (Fe_7S_8) and their use in estimating paleotemperatures. *Earth and Planetary Science Letters* 176:107–116.

Elbra T., Kontny A., Pesonen L. J., Schleifer N., and Schell C. 2007. Petrophysical and paleomagnetic data of drill cores from the Bosumtwi impact structure, Ghana. *Meteoritics & Planetary Science* 42. This issue.

Ellwood B. B., Burkart B., Rajeshwar K., and Darwin R. 1989. Are the iron carbonate minerals ankerite and ferroan dolomite, like siderite, important in paleomagnetism? *Journal of Geophysical Research* 94:7321–7331.

Franken D., Bosum W., and Wohlenberg J. 1985. A geological and geophysical interpretation of the magnetic anomaly of Lammersdorf, Hohes Venn (West Germany). *Neues Jahrbuch für Geologie und Paläontologie, Abhandlungen* 171:363–375.

Hart R. J., Hargraves R. B., Andreoli M. A. G., Tredoux M., and Doucoure C. M. 1995. Magnetic anomaly near the center of the Vredefort structure: Implications for impact-related magnetic signatures. *Geology* 23:277–280.

Hirdes W., Davis D. W., Lüdtke G., and Konan G. 1996. Two generations of Birmian (Paleoproterozoic) volcanic belts in notheastern Côte d'Ivoire (West Africa): Consequences for the "Birmian controversy." *Precambrian Reseach* 80:173–191.

Hrouda F. 1994. A technique for the measurement of thermal changes of magnetic susceptibility of weakly magnetic rocks by the CS-2 apparatus and KLY-2 kappabridge. *Geophysical Journal International* 118:604–612.

Hunt C. P., Moskowitz B. M., and Banerjee S. K. 1995. Magnetic properties of rocks and minerals. In *Rock physics and phase relations: A handbook of physical constants*, edited by Ahrens T. AGU Reference Shelf, vol. 3. Washington, D.C.: American Geophysical Union. pp. 189–204.

Jones W. B., Bacon M., and Hastings D. A. 1981. The Lake Bosumtwi impact crater, Ghana. *Geological Society of America Bulletin* 92:342–349.

Jover O., Rochette P., Lorand J. P., Maeder M., and Bouchez J. L. 1989. Magnetic mineralogy of some granites from the French Massif Central: Origin of their low-field susceptibility. *Physics of the Earth and Planetary Interiors* 55:79–92.

Just J. 2005. Modification of magnetic properties in granite during hydrothermal alteration (EPS-1 borehole, Upper Rhine Graben). Ph.D. thesis, University of Heidelberg, Heidelberg, Germany.

Karp T., Artemieva N., and Milkereit B. 2004. Pre-drilling investigation of the Lake Bosumtwi impact crater: Constraints from geophysics and numerical modeling (abstract #1282). 35th Lunar and Planetary Science Conference. CD-ROM.

Kissin S. A. and Scott S. D. 1982. Phase relations involving pyrrhotite below 350 °C. *Economic Geology* 77:1739–1754.

Kletetschka G., Wasilewski P. J., and Taylor P. T. 2000. Unique thermoremanent magnetization of multidomain sized hematite: Implications for magnetic anomalies. *Earth and Planetary Science Letters* 176:469–479.

Kletetschka G., Acuna M. H., Kohout T., Wasilewski P. J., and Connerney J. E. P. 2004. An empirical scaling law for acquisition of thermoremanent magnetization. *Earth and Planetary Science Letters* 226:521–528.

Koeberl C., Bottomley R., Glass B. P., and Storzer D. 1997. Geochemistry and age of Ivory Coast tektites and microtektites. *Geochimica et Cosmochimica Acta* 61:1745–1772.

Koeberl C., Milkereit B., Overpeck J. T., Scholz C. A., Reimold W. U., Amoako P. Y. O., Boamah D., Claeys P., Danuor S., Deutsch A., Hecky R. E., King J., Newsom H., Peck J., and Schmitt D. R. 2006. An international and multidisciplinary drilling project into a young complex impact structure: The 2004 ICDP Bosumtwi impact crater, Ghana, drilling project—An overview (abstract #1859). 37th Lunar and Planetary Science Conference. CD-ROM.

Koeberl C., Milkereit B., Overpeck J. T., Scholz C. A., Amoako P. Y. O., Boamah D., Danuor S., Karp T., Kueck J., Hecky R. E., King J. W., and Peck J. A. 2007. An international and multidisciplinary drilling project into a young complex impact structure: The 2004 ICDP Bosumtwi Crater Drilling Project—An overview. *Meteoritics & Planetary Science* 42. This issue.

Kontny A., Friedrich G., Behr H. J., De Wall H., Horn E. E., Möller P., and Zulauf G. 1997. Formation of ore minerals in metamorphic rocks of the German continental deep drilling site (KTB). *Journal of Geophysical Research* 102:18,323–18,336.

Kontny A., De Wall H., Sharp T. G., and Pósfai M. 2000. Mineralogy and magnetic behavior of pyrrhotite from a 260 °C section at the KTB drilling site, Germany. *American Mineralogist* 85:1416–1427.

Langenhorst F., Pesonen L. J., Deutsch A., and Hornemann U. 1999. Shock experiments on diabase: Microstructural and magnetic properties (abstract #1241). 30th Lunar and Planetary Science Conference. CD-ROM.

Morrow J. R. 2006. Petrographic characteristics of quartz in suevitic impact breccia, drill core LB-07A (abstract # 1258). 37th Lunar and Planetary Science Conference. CD-ROM.

Muxworthy A. R. 1999. Low-temperature susceptibility and

hysteresis of magnetite. *Earth and Planetary Science Letters* 169:51–58.

Nakazawa H. and Morimoto N. 1971. Phase relations and superstructures of pyrrhotite, Fe1-xS. *Material Research Bulletin* 6:345–358.

Nakazawa H., Morimoto N., and Watanabe E. 1975. Direct observation of metal vacancies by high-resolution electron microscopy. Part I: 4C type pyrrhotite (Fe_7S_8). *American Mineralogist* 60:359–366.

Pesonen L. J., Marcos N., and Pipping F. 1992. Paleomagnetism of the Lappajärvi impact structure, western Finland. *Tectonophysics* 216:123–142.

Pesonen L. J., Deutsch A., Hornemann U., and Langenhorst F. 1997. Magnetic properties of diabase samples shocked experimentally in the 4.5 to 35 GPa range. Proceedings, 28th Lunar and Planetary Science Conference. pp. 1087–1088.

Pesonen L. J., Koeberl C., and Hautaniemi H. 2003. Airborne geophysical survey of the Lake Bosumtwi meteorite impact structure (southern Ghana)—Geophysical maps with descriptions. *Jahrbuch der Geologischen Bundesanstalt, Vienna (Yearbook of the Austrian Geological Survey)* 143:581–604.

Pilkington M. and Grieve R. A. F. 1992. The geophysical signature of terrestrial impact craters. *Reviews of Geophysics* 30:161–181.

Plado J., Pesonen L. J., Koeberl C., and Elo S. 2000. The Bosumtwi meteorite impact structure, Ghana: A magnetic model. *Meteoritics & Planetary Science* 35:723–732.

Pósfai M., Sharp T. G., and Kontny A. 2000. Pyrrhotite varieties from the 9.1 km deep borehole of the KTB project. *American Mineralogist* 85:1406–1415.

Pucher R. 1994. Pyrrhotite-induced aeromagnetic anomalies in western Germany. *Journal of Applied Geophysics* 32:33–42.

Reimold W. U., Coney L., Koeberl C., and Gibson R. L. 2006. ICDP borehole LB-07A (Bosumtwi impact structure, Ghana): An overview and first multidisciplinary results (abstract #1350). 37th Lunar and Planetary Science Conference. CD-ROM.

Rochette P., Fillion G., Mattéi J. L., and Dekkers M. J. 1990. Magnetic transition at 30–34 Kelvin in pyrrhotite: Insight into a widespread occurrence of this mineral in rocks. *Earth and Planetary Science Letters* 98:319–328.

Rochette P., Fillion G., Ballou R., Brunet F., Ouladdiaf B., and Hood L. 2003. High-pressure magnetic transition in pyrrhotite and impact demagnetization on Mars. *Geophysical Research Letters* 30, doi: 10.1029/2003GL017359.

Rochette P., Gattacceca J., Chevrier V., Hoffmann V., Lorand J. P., Funaki M., and Hochleitner R. 2005. Matching Martian crustal magnetization and magnetic properties of Martian meteorites. *Meteoritics & Planetary Science* 40:529–540.

Scholz C. A., Karp T., Brooks K. M., Milkereit B., Amoako P., and Arko J. 2002. Pronounced central uplift identified in the Bosumtwi impact structure, Ghana, using multichannel seismic reflection data. *Geology* 30:939–942.

Soffel H. C. 1977. Pseudo-single-domain effects and single-domain multidomain transition in natural pyrrhotite deduced from domain structure observations. *Journal of Geophysics* 42:351–359.

Soffel H. C. 1981. Domain structure of natural fine-grained pyrrhotite in a rock matrix (diabase). *Physics of the Earth and Planetary Interiors* 26:98–106.

Taylor P. N., Moorbath S., Leube A., and Hirdes W. 1992. Early Proterozoic crustal evolution in the Birmian of Ghana: Constraints from geochronology and isotope geochemistry. *Precambrian Research* 56:97–111.

Trepmann C. A. and Spray J. G. 2006. Shock-induced crystal-plastic deformation and post-shock annealing of quartz: Microstructural evidence from crystalline target rocks of the Charlevoix impact structure, Canada. *European Journal of Mineralogy* 18:161–173.

Ugalde H. A., Artemieva N., and Milkereit B. 2005. Magnetization on impact structures—Constraints from numerical modeling and petrophysics. *In Large meteorite impacts III*, edited by Deutsch A., Hörz F., and Kenkmann T. GSA Special Paper #384. Boulder, Colorado: Geological Society of America. pp. 25–42.

Ugalde H. A., Morris W. A., and Danuor S. K. 2006. 3-D vector magnetics at Lake Bosumtwi: Experiment and results (abstract #1064). 37th Lunar and Planetary Science Conference. CD-ROM.

Ugalde H., Morris W. A., Clark C., Miles B., and Milkereit B. 2007a. The Lake Bosumtwi meteorite impact structure, Ghana—A magnetic image from a third observational level. *Meteoritics & Planetary Science* 42. This issue.

Ugalde H., Morris W. A., Pesonen L. J., and Danour S. K. 2007b. The Lake Bosumtwi meteorite impact structure, Ghana—Where is the magnetic source? *Meteoritics & Planetary Science* 42. This issue.

Vahle C. and Kontny A. 2005. The use of field dependence of AC susceptibility for the interpretation of magnetic mineralogy and magnetic fabrics in the HSDP-2 basalts, Hawaii. *Earth and Planetary Science Letters* 238:110–129.

Wippern J. 1986. Gesteinsmagnetische Untersuchungen an Pyrrhotin-haltigen Bohrkernen. Master's thesis, University of München, Munich, Germany.

Worm H. U., Clark D., and Dekkers M. J. 1993. Magnetic susceptibility of pyrrhotite: grain size, field and frequency dependence. *Geophysical Journal International* 114:127–137.